JCI insight

RESEARCH ARTICLE

Dysregulated NK cell PLCγ2 signaling and activity in juvenile dermatomyositis

Allison A. Throm,[1,2] Joshua B. Alinger,[1] Jeanette T. Pingel,[1] Allyssa L. Daugherty,[1] Lauren M. Pachman,[3,4] and Anthony R. French[1,2]

[1]Division of Pediatric Rheumatology, Department of Pediatrics, Washington University School of Medicine, St. Louis, Missouri, USA. [2]Department of Biomedical Engineering, Washington University, St. Louis, Missouri, USA. [3]Department of Pediatrics, Northwestern University Feinberg School of Medicine, Chicago, Illinois, USA. [4]Stanley Manne Children's Research Institute, Cure JM Center of Excellence in Juvenile Myositis Research, Department of Pediatrics, Ann & Robert H. Lurie Children's Hospital of Chicago, Chicago, Illinois, USA.

Juvenile dermatomyositis (JDM) is a debilitating pediatric autoimmune disease manifesting with characteristic rash and muscle weakness. To delineate signaling abnormalities in JDM, mass cytometry was performed with PBMCs from treatment-naive JDM patients and controls. NK cell percentages were lower while frequencies of naive B cells and naive CD4$^+$ T cells were higher in JDM patients than in controls. These cell frequency differences were attenuated with cessation of active disease. A large number of signaling differences were identified in treatment-naive JDM patients compared with controls. Classification models incorporating feature selection demonstrated that differences in phospholipase Cγ2 (PLCγ2) phosphorylation comprised 10 of 12 features (i.e., phosphoprotein in a specific immune cell subset) distinguishing the 2 groups. Because NK cells represented 5 of these 12 features, further studies focused on the PLCγ2 pathway in NK cells, which is responsible for stimulating calcium flux and cytotoxic granule movement. No differences were detected in upstream signaling or total PLCγ2 protein levels. Hypophosphorylation of PLCγ2 and downstream mitogen-activated protein kinase-activated protein kinase 2 were partially attenuated with cessation of active disease. PLCγ2 hypophosphorylation in treatment-naive JDM patients resulted in decreased calcium flux. The identification of dysregulation of PLCγ2 phosphorylation and decreased calcium flux in NK cells provides potential mechanistic insight into JDM pathogenesis.

Introduction

Juvenile dermatomyositis (JDM) is an inflammatory myopathy/vasculopathy that results in inflammation of striated muscle, skin, and the gastrointestinal tract. It presents with characteristic skin findings (including heliotrope rash, Gottron's papules, and periungual erythema and telangiectasias) and proximal muscle weakness in childhood, with an incidence of 2–3 cases per million children (1). Before the advent of steroid therapy, JDM had a mortality rate of 40% (1). Even with treatment, the disease inflicts significant morbidity on children, with over 25% of JDM patients experiencing persistent symptoms for over 36 months (2) and approximately 20% of patients experiencing an even more protracted, refractory disease course (1).

The etiology of JDM is not well characterized, but both adaptive and innate immune responses have been associated with JDM pathogenesis. Myositis-specific and myositis-associated antibodies (against extractable nuclear antigens) have been identified in approximately 65% of JDM patients (3, 4). Furthermore, B cell depletion with rituximab (a chimeric monoclonal antibody against CD20) leads to clinical improvement in some JDM patients (5–7). T cells are implicated by the association of JDM with HLA-B08 and HLA-DRB1 (8–10). Furthermore, JDM patients exhibit increased skewing toward CXCR5$^+$ Th2 and Th17 T cell subsets, which correlates with disease activity and blood plasmablasts (11). The innate immune system also appears to play a role in JDM. Plasmacytoid dendritic cells and macrophage-secreted proteins are present in inflamed JDM patient muscles (12, 13), and chemokines eotaxin, monocyte chemoattractant protein-1, and IFN-γ–induced protein 10 are elevated in JDM patient serum in comparison with healthy controls (14). In addition, specific TNF and IL-1 alleles as well as a type I IFN–stimulated gene signature are associated with JDM disease risk (15, 16).

Conflict of interest: The authors have declared that no conflict of interest exists.

Submitted: June 28, 2018
Accepted: October 16, 2018
Published: November 15, 2018

Reference information:
JCI Insight. 2018;3(22):e123236.
https://doi.org/10.1172/jci.insight.123236.

Several studies have implicated NK cells in the pathogenesis of JDM. NK cells are innate lymphocytes (defined as $CD3^{-}CD56^{+}$) with germline-encoded receptors that play a critical role in antiviral defense and tumor surveillance (17, 18). NK cells perform this critical function by secreting immunomodulatory cytokines and releasing cytotoxic granules to lyse target cells (19). The movement of cytotoxic granules within NK cells is regulated by the phosphorylation of phospholipase Cγ2 (PLCγ2) and subsequent generation of calcium flux (20–22). There is accumulating evidence that human NK cells play an immunoregulatory role and that NK cell dysfunction may contribute to the onset of human autoimmunity (23, 24). Despite some experimental limitations, several previous JDM studies have reported evidence of decreased NK cell percentages in the blood of treatment-naive patients compared with controls (25), a weak association between increased NK cell percentages in the blood and decreased JDM disease activity (26), and data suggestive of NK cells infiltrating the affected muscle in JDM patients (15). Furthermore, decreased NK cell cytotoxicity in JDM has been reported in a small cohort of 5 JDM patients (27) and in 2 additional treatment-naive JDM patients (28).

Despite these insights, the etiology of JDM is not well understood, and the dysregulation of immune cell signaling in JDM has not been systematically investigated. Therefore, to delineate potential immune cell signaling abnormalities in JDM, we performed mass cytometry on PBMCs from treatment-naive JDM patients and controls. By pairing the deep profiling facilitated by mass cytometry with phospho-specific antibodies, we were able to probe the activation state of 14 signaling molecules in 23 distinct leukocyte subsets within single-patient samples, both at baseline and over a time course following stimulation with a cocktail of cytokines and cross-linking antibodies. This approach identified dysregulated PLCγ2 phosphorylation in several immune cell types, with defective PLCγ2 phosphorylation in NK cells comprising the primary signaling difference between treatment-naive JDM patients and controls.

Results

Patient cohort. Samples from 17 treatment-naive JDM patients, 11 of these 17 JDM patients after achieving clinically inactive disease, and 17 healthy controls were analyzed (Table 1). The mean age of the patients and the controls in the cohort were 7.4 years and 9.3 years, respectively, with similar sex distributions (76% and 70.6% girls in patients and controls, respectively). Eighty-two percent of the patients were White (compared with 70.6% of the controls). The median duration of untreated disease in the patients was 3.6 months (average 5.6 months with a standard deviation of 5 months).

Cell percentages. Mass cytometry was used to quantify the distribution of 23 distinct leukocyte subsets in samples from treatment-naive JDM patients, healthy controls, and a subset of the JDM patients after achieving clinically inactive disease. Samples were gated on live immune cell singlets and then into 23 immune cell types, based on distribution of surface markers (Supplemental Figure 1; supplemental material available online with this article; https://doi.org/10.1172/jci.insight.123236DS1). NK cells were present at a lower frequency while the percentages of naive B cells and naive $CD4^{+}$ T cells were higher in treatment-naive JDM patients than in controls (Figure 1A). Frequency of PBMC subsets was also examined in 11 paired treatment-naive and clinically inactive JDM patient samples. Naive B cell frequency normalized in paired samples with cessation of active disease (Figure 1B). Although there was a trend toward increased NK cell percentages with cessation of active disease in paired samples (with increased NK cell percentages in 9 of the 11 paired samples), the difference was not statistically significant after multiple hypothesis correction (Figure 1B; t = 2.37, degrees of freedom [df] = 10, P = 0.039). However, there was no statistically significant difference in NK cell percentages between the samples from JDM patients with clinically inactive disease and healthy controls (mean ± standard deviation of 6.00 ± 2.89 and 7.60 ± 5.42 for the JDM patients with clinically inactive disease and healthy controls, respectively; t = 1.04, df = 26, P = 0.310), supporting the trend toward normalization in NK cell percentages with cessation of active disease.

Signaling phenotype. Differences in signaling between treatment-naive JDM patients and controls (or patients with clinically inactive disease) were also examined. To simultaneously gain insights about multiple signaling pathways, samples were stimulated concurrently with IL-2, IL-12, LPS, and IFN-α4 as well as IgM, CD3, and CD16 cross-linking for 0, 3, or 15 minutes and then subjected to mass cytometry to quantify phosphorylation of a panel of 14 intracellular signaling molecules (Supplemental Table 1). Because 292 stratifying (i.e., distinguishing) features were detected when significance analysis of microarrays (SAM) was used to compare JDM patients and controls (data not shown), a method incorporating feature selection was necessary to aid in interpreting the results. Feature selection techniques, such as least absolute

Table 1. Patient demographics

Patient	Sex	Race	Duration of untreated disease (months)	Age at sample collection (yrs)	Age at clinically inactive disease sample collection (yrs)	Medications in clinically inactive dis. sample	MSA	MAA	Healthy control	Site
1	F	W	2	7.2	9.3	MTX	anti-SAE	negative	11.2 yr W F	1
2	M	W	3	3.2	5.1	MTX, IVIG	negative	negative	2.6 yr W M	1
3	M	W	1	9.1	10	MTX, IVIG, PLQ	p155/140	negative	7.5 yr W M	1
4	F	W	12	16.3			p155/140	negative	13.4 yr W F	1
5	F	W	<1	12.8			MJ	negative	12.6 yr W F	1
6	F	W	<3	8.2			p155/140	negative	11.2 yr B F	1
7	M	W	4	12.1			MDA5	negative	15.7 yr B M	1
8	F	W	6	4.2	8.2		p155/140	negative	4.1 yr W M	2
9	M	H	19	3			p155/140	negative	6.5 yr W M	2
10	F	W	<4	9.7	14.9		Mi-2	negative	9.3 yr W M	2
11	F	B	6	8.2	12.9		negative	negative	11 yr NA/H F	2
12	F	W	3	5.5	7.3	PO, MTX, IVIG, MMF	p155/140	Ro	7.1 yr W F	2
13	F	W/A	2	3.2	7.1		negative	negative	8.8 yr W F	2
14	F	B	2	6.3	15.6	MTX, CSA, MMF	Mi-2, p155/140	negative	11 yr W F	2
15	F	W	13	9.6	16.0		p155/140	Ro	13 yr W F	2
16	F	W	8	5.2	15.0		p155/140	negative	6 yr NA/H F	2
17	F	W	6	2.3			negative	negative	7 yr W/H F	2

Research site 1 denotes St. Louis Children's Hospital, and research site 2 denotes Lurie Children's Hospital. If not noted, patient was not on medication at the time of clinically inactive disease sample collection. Medication abbreviations: MSA, myositis-specific autoantibody; MAA, myositis-associated autoantibody; SAE, small ubiquitin-like modifier (SUMO) activating enzyme; PO, oral prednisone; MTX, methotrexate; IVIG, intravenous immunoglobulin; PLQ, plaquenil; MJ, also known as nuclear matrix protein 2 (NXP-2) CSA, cyclosporine; MMF, mycophenolate mofetil. Abbreviations for race: W, White; B, African American; H, Hispanic; A, Asian.

shrinkage and selection operator (LASSO), enhance generalization by reducing overfitting and removing redundant or irrelevant features (e.g., features that are redundant in the presence of another correlated feature; ref. 29). Cluster identification, characterization, and regression (Citrus), a technique that combines unsupervised hierarchical clustering with a regularized supervised learning algorithm to predict the class of the samples (e.g., patients versus controls) from the features of a data set (e.g., phosphorylation of a signaling molecule in an immune subset/cluster), with LASSO regression was used to determine which features were stratifying between treatment-naive JDM patients and controls (30, 31). This approach identified NK cell subsets as stratifying for each stimulation time point as well as unstimulated classical monocytes and T cells (Figure 2A). The 12 stratifying features Citrus identified (unstimulated as well as 3- and 15-minute–stimulated p-PLCγ2 in NK cell clusters, unstimulated p-STAT3 in a subset of NK cells, unstimulated p-PLCγ2 in a classical monocyte subset, unstimulated as well as 3- and 15-minute–stimulated p-PLCγ2 in $CD4^+$ and $CD8^+$ T cell clusters, and 3-minute–stimulated p-STAT3 in nonclassical monocytes) were sufficient to completely segregate treatment-naive JDM patient samples from control samples by hierarchical clustering (Figure 2B).

A partial least squares discriminant analysis (PLS-DA) model was constructed from the selected features to visualize the stratifying signaling features in relation to classification as patient or control (Figure 2, C and D). PLS-DA was used to decompose matrices of signaling data and disease state into scores and loadings matrices, with the hypothesis that the classification of a sample as a treatment-naive patient or control is dependent upon the signaling profile of the sample. The scores plot describes the relationship of the samples to one another (Figure 2C), and the loadings plot describes the relationships of the variables (signaling protein phosphorylation in specific immune cell clusters) to one another (Figure 2D). The PLS-DA model was able to completely distinguish patients and controls (Figure 2C). Furthermore, the loadings plot demonstrated that treatment-naive JDM patient samples were associated with lower levels of NK cell p-PLCγ2 for all stimulation time points (and unstimulated classical monocyte p-PLCγ2) in comparison with control samples, while p-PLCγ2 in stratifying T cell clusters and p-STAT3 in NK cell and nonclassical monocyte clusters were higher in treatment-naive JDM patient samples than in controls (Figure 2D). PLCγ2 signaling

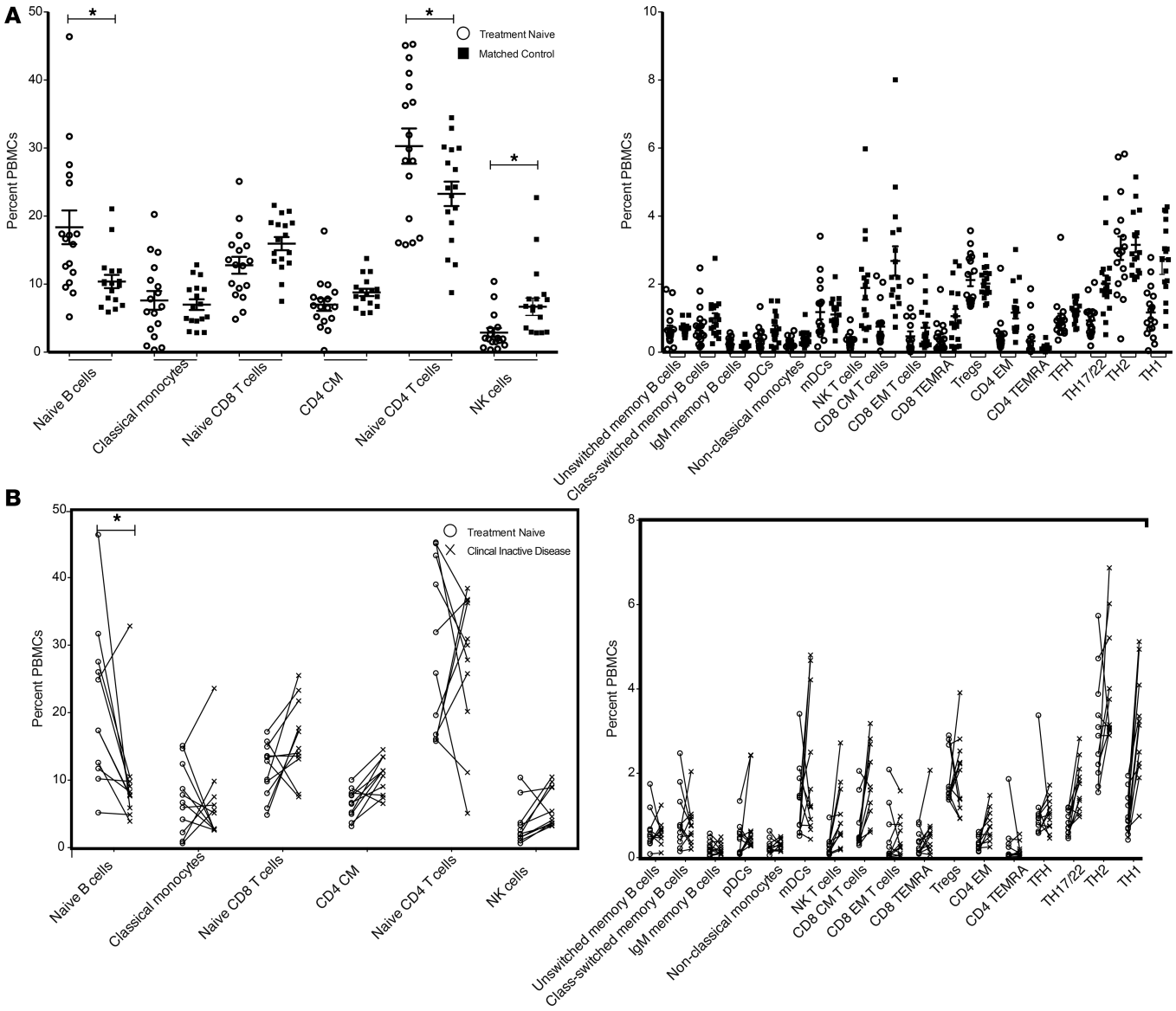

Figure 1. PBMC percentages in JDM patients and healthy controls. Open circles denote treatment-naive patients (n = 17). Filled squares denote healthy controls (n = 17). (**A**) Percentage of PBMC population in treatment-naive patients and controls for higher frequency (left panel) and lower frequency (right panel) immune cell types (1-way ANOVA: F = 7.429, P < 0.001; naive B cells: t = 7.459, P < 0.05; naive CD4$^+$ T cells: t = 6.561, P < 0.05; NK cells: t = 4.415, P < 0.05). (**B**) Percentage of PBMC populations in paired treatment-naive and clinically inactive disease patient samples for higher frequency (left panel) and lower frequency (right panel) immune cell types (1-way ANOVA: F = 36.15, P < 0.005; naive B cells: t = 6.986, P < 0.05, and n = 11 paired patient samples). ×'s denote patients after achieving clinically inactive disease (n = 11). Error bars represent the mean ± SEM. *P < 0.05 after appropriate multiple hypothesis correction.

dysregulation was also detected in bulk (manually gated) immune cell populations corresponding to the observation in the immune cell subsets represented by the Citrus clusters (Supplemental Figures 6 and 7).

Given that many of the detected stratifying differences were in NK cells (5 of 12 Citrus features) and PLCγ2 (10 of 12 Citrus features) (Figure 2D), we confirmed the significance of NK cell PLCγ2 phosphorylation using 2-tailed Welch's t tests with stringent Bonferroni correction to account for 897 comparisons (299 features examined for each of the 3 time points). This statistical test specified that the 3 most significant features (phosphoprotein in a specific immune cell subset) were NK cell p-PLCγ2 at 0, 3, and 15 minutes (Supplemental Table 2) and that 7 of the 9 features involved p-PLCγ2 and 1 involved phosphorylated MAPK-activated protein kinase 2 (p-MAPKAPK2), a downstream kinase in the PLCγ2 signaling cascade (Supplemental Table 2), clearly highlighting the importance of dysregulated NK cell p-PLCγ2 in JDM. Therefore, subsequent studies focused on NK cell PLCγ2 signaling.

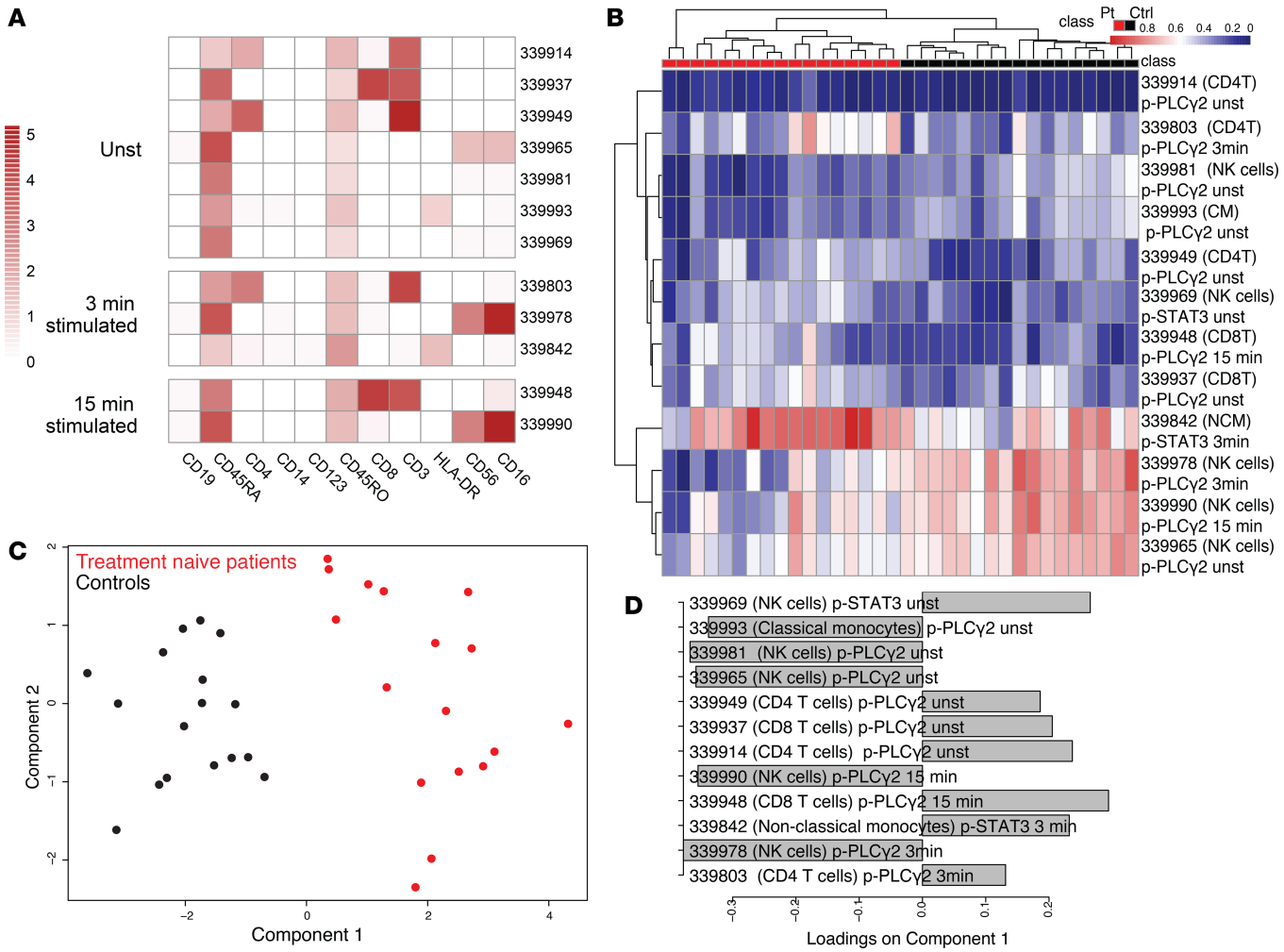

Figure 2. Signaling molecules in several immune cell subsets were stratifying between treatment-naive JDM patients and healthy controls for unstimulated as well as 3- and 15-minute–stimulated samples. Citrus was used to identify stratifying clusters (n = 17 treatment-naive patients, n = 17 matched controls in all subpanels). (**A**) Heatmap of arcsinh median intensity for surface markers used for Citrus clustering for stratifying clusters detected by Citrus at all time points (cluster numbers are denoted on the right side of the figure). Unst: unstimulated. (**B**) Heatmap of arcsinh-transformed median signaling molecule intensity of stratifying signaling molecules in the respective clusters for all time points retained by LASSO feature selection with the minimum cross-validation error as the threshold. Rows correspond to signaling features, and columns correspond to samples, with red denoting treatment-naive patients and black representing healthy controls. Pt: patient; CM: classical monocytes; CD4T: $CD4^+$ T cells; CD8T: $CD8^+$ T cells; NCM: nonclassical monocytes. (**C**) PLS-DA scores plot for classification of treatment-naive patients and controls developed using LASSO-selected features from Citrus in (**B**). Red points correspond to treatment-naive patients and black to controls. (**D**) PLS-DA loadings plot (depiction of relationship of variables to one another in dimensionally reduced variable space) for classification of treatment-naive patients and controls developed using LASSO-selected features from Citrus in (**B**).

NK cell PLCγ2 signaling cascade. The NK cell signaling time course was examined for phosphorylation of PLCγ2 as well as of 2 kinases upstream of PLCγ2 (spleen tyrosine kinase [Syk]/zeta-chain-associated protein kinase 70 [ZAP70], IL-2–inducible T cell kinase [Itk]/Bruton's tyrosine kinase [Btk]) and a downstream kinase (MAPKAPK2) in the PLCγ2 signaling cascade. NK cell PLCγ2 phosphorylation was lower in treatment-naive JDM patients than controls for all time points (Figure 3A, manually gated on NK cells). Interestingly, available samples for a subset (n = 11) of these JDM patients while in a clinically inactive disease state (note that 5 of the 11 patients with clinically inactive disease were on medications) displayed an intermediate time course between treatment-naive JDM patients and controls (Supplemental Figure 3A), suggesting that the observed phosphorylation differences are not likely due to germline mutations in PLCγ2. No statistically significant differences were observed in the phosphorylation of upstream signaling molecules Syk/ZAP70 or Itk/Btk in NK cells between treatment-naive JDM patients and controls (Figure 3, B and C). Phosphorylation of the downstream kinase MAPKAPK2 was lower in treatment-naive JDM patients, similar to what was seen with p-PLCγ2 (Figure 3D).

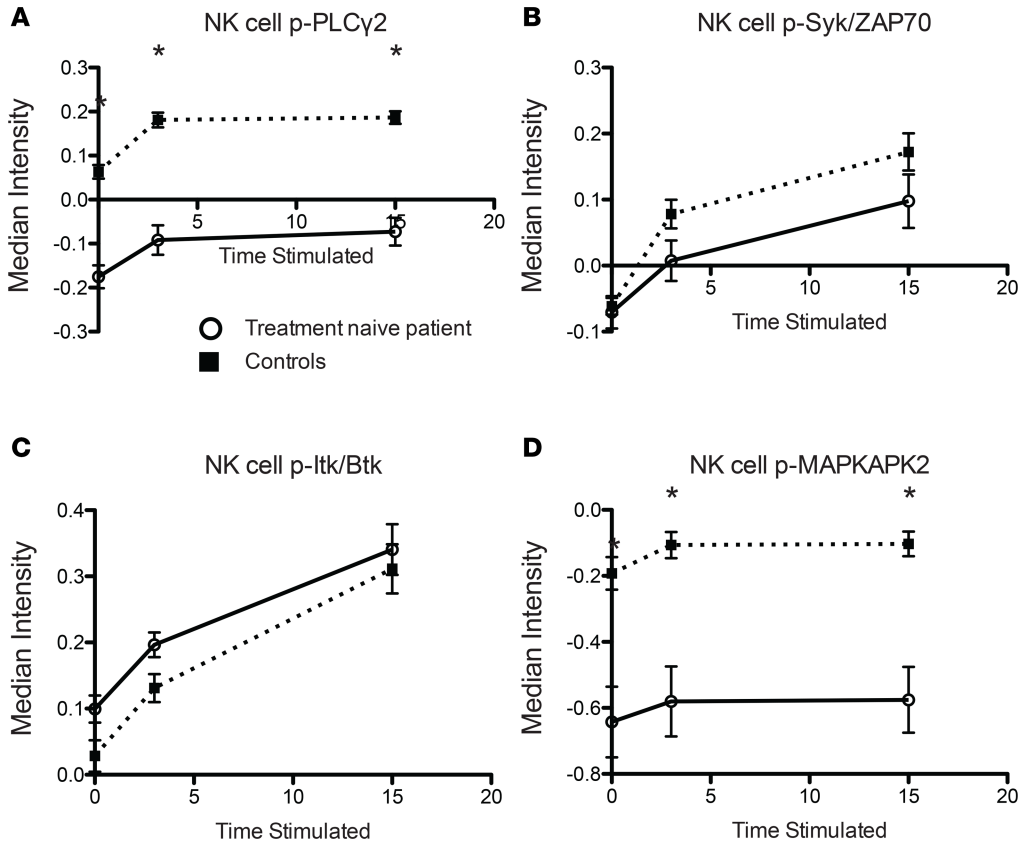

Figure 3. Treatment-naive JDM patient NK cells hypophosphorylate PLCγ2 and MAPKAPK2 but not Syk/ZAP70 and Itk/Btk in comparison with controls over stimulation time course (tested with 2-way Welch's *t* tests with Benjamini-Hochberg multiple hypothesis correction for 12 tests). Open circles denote treatment-naive patients (n = 17). Filled squares denote healthy controls (n = 17). Data are displayed as the arcsinh ratio of the median intensity of the sample normalized to the run control. (**A**) NK cell PLCγ2 (0-min $P = 6.88 \times 10^{-8}$, 3-min $P = 1.62 \times 10^{-6}$, and 15-min $P = 1.47 \times 10^{-6}$) phosphorylation differs between treatment-naive JDM patients and controls. (**B**) NK cell Syk/ZAP70 and (**C**) Itk/Btk phosphorylation are not different between treatment-naive JDM patients and controls. (**D**) MAPKAPK2 (0-min $P = 0.003$, 3-min $P = 0.002$, and 15-min $P = 0.0008$) phosphorylation differs over the time course between 17 treatment-naive JDM patients and 17 controls. Error bars represent the mean ± SEM. *$P < 0.05$.

Given that differences were detected in NK cell PLCγ2 phosphorylation kinetics, we examined several potential mechanisms for this hypophosphorylation. Flow cytometry was performed with available remaining samples from 3 treatment-naive JDM patients and controls to assess NK cell levels of PLCγ2 protein as well as total phosphatidylinositol-3,4,5-trisphosphate 5-phosphatase 1 (SHIP1) protein, an inhibitory molecule in the PLCγ2 signaling cascade (Figure 4). No significant difference was detected in total protein levels of PLCγ2 (Figure 4A), suggesting that PLCγ2 hypophosphorylation in JDM patient NK cells was not simply due to lower PLCγ2 expression levels. Unexpectedly, SHIP1 protein levels were lower in treatment-naive JDM patients than in controls (Figure 4B).

PLCγ2 is a key signaling component downstream of many NK cell receptors, including CD16, 2B4, and NKG2D. CD16 cross-linking in our stimulation cocktail was upstream of the observed phosphorylation of PLCγ2 in NK cells; therefore, it was of interest to determine if CD16 receptor expression levels differed between treatment-naive patients and controls. CD16 expression was indeed significantly lower in treatment-naive JDM patients in comparison with controls (Figure 4C). Given the observed variation in treatment-naive patient NK cell CD16 expression, p-PLCγ2 integrated over time (i.e., the area under the p-PLCγ2 signal-versus-time plot, a metric that captures the duration and magnitude of p-PLCγ2 signaling; ref. 32) was plotted versus CD16 expression levels (arcsinh MFI of CD16), demonstrating a significantly positive correlation with the p-PLCγ2 integrated time course in treatment-naive patients but not healthy controls or patients with clinically inactive disease (Figure 4D and Supplemental Figure 4). Patients with clinically inactive disease displayed an intermediate slope between treatment-naive patients and controls.

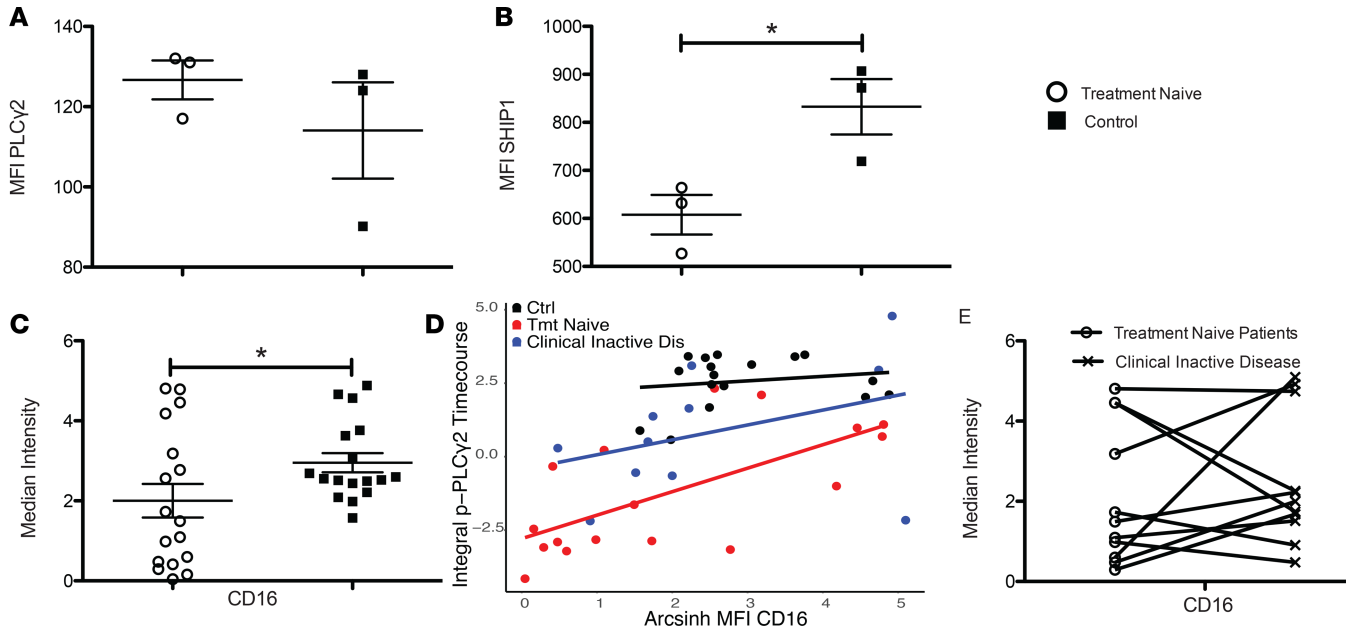

Figure 4. Evaluation of total PLCγ2, SHIP1, and CD16 levels. Open circles denote treatment-naive patients. Filled squares denote healthy controls. (**A**) Total PLCγ2 protein levels determined with flow cytometry (n = 3 treatment-naive patients, n = 3 controls; 2-way Welch's t test: t = 1.662, df = 4, P = 0.1719). (**B**) Total SHIP1 protein levels determined with flow cytometry (n = 3 treatment-naive patients, n = 3 controls; 2-way Welch's t test: t = 3.701, df = 4, P = 0.0208). (**C**) Arcsinh transformation of CD16 in treatment-naive JDM patient (open circles) and control (filled squares) NK cells assessed with mass cytometry (1-way Welch's t test: t = 1.968, df = 25, P = 0.0301, n = 17 patients, and n = 17 controls). (**D**) Correlation of integrated p-PLCγ2 time course versus arcsinh MFI CD16 for patients and controls (treatment-naive patients: $y = -2.78 + 0.80x$, r = 0.66, P = 0.0039, and n = 17; patients with clinically inactive disease: $y = -0.44 + 0.568x$, r = 0.38, P = 0.254, and n = 11; controls: $y = 2.12 + 0.15x$, r = 0.17, P = 0.51, n = 17). Tmt: treatment; Dis: disease. (**E**) Arcsinh transformation of CD16 in NK cells from treatment-naive JDM patients (open circles) and paired JDM patients with clinically inactive disease (×'s) (1-way paired Welch's t test: t = 1.343, df = 10, P = 0.209, n = 11 treatment-naive patients, and n = 11 patients with clinically inactive disease). Error bars represent the mean ± SEM. *$P < 0.05$.

The positive correlation of CD16 expression levels with PLCγ2 signaling over time in treatment-naive patient NK cells could suggest that lower p-PLCγ2 signaling was due to decreased CD16 receptor expression levels; however, the normal phosphorylation of the 2 upstream kinases (Syk/ZAP70 and Itk/Btk) that lie between CD16 and PLCγ2 suggests that the lower CD16 levels are correlative but not causative.

Impact of lower NK cell p-PLCγ2. As an assessment of the functional consequences of lower p-PLCγ2 levels, calcium flux was evaluated by flow cytometry in enriched NK cells from available samples from 2 treatment-naive JDM patients and 1 healthy control. The treatment-naive JDM patients displayed suppressed calcium flux following 2B4 and NKG2D receptor cross-linking in comparison with the healthy control (Figure 5A). Expression levels of 2B4 and NKG2D did not differ between the treatment-naive JDM patients and control (Figure 5, B and C), verifying that the diminished calcium flux was not due to decreased NK cell–activating receptor levels. The reduced calcium flux demonstrated that the hypophosphorylation of PLCγ2 has functional consequences and strongly suggests that NK cell granule movement and cytotoxicity would be impaired in treatment-naive JDM patients.

Finally, median signaling intensities of CD69 and Ki-67 (normalized to the run control by the arcsinh ratio) were also evaluated in samples as surrogates for cellular activation and proliferation. Treatment-naive JDM patients' NK cells were more activated than control cells, as assessed by median levels of normalized CD69 intensity (Supplemental Figure 5A). Furthermore, treatment-naive JDM patients' NK cells were actively proliferating more than control NK cells, as demonstrated by normalized median intensity of Ki-67 (Supplemental Figure 5B).

Discussion

Based on the hypothesis that cell signaling differences (particularly in innate leukocytes) may contribute to early disease in JDM, this study was designed to delineate signaling differences in peripheral immune cell subsets between treatment-naive JDM patients and controls using the high-dimensional capabilities of mass cytometry coupled with phospho-specific antibodies. Many differences were detected; however, using

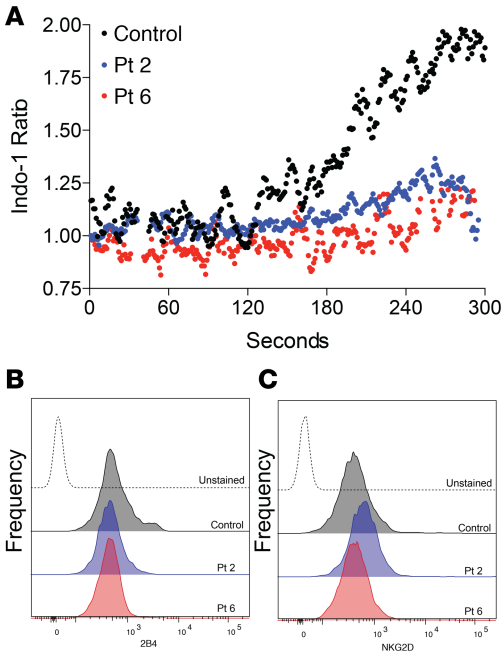

Figure 5. Enriched NK cells from treatment-naive JDM patients exhibit decreased Ca^{2+} flux compared with NK cells from healthy controls upon stimulation by 2B4 and NKG2D receptor cross-linking. (**A**) Calcium flux in treatment-naive patient and control NK cells (n = 2 treatment-naive patients, n = 1 matched control). The cell surface expression of 2B4 (**B**) and NKG2D (**C**) was similar in the treatment-naive JDM patients and controls.

several analysis approaches (including Citrus with LASSO feature selection), signaling differences that were sufficient to differentiate between JDM patients and controls were found to primarily involve the phosphorylation of PLCγ2 in NK cells as well as in classical monocytes, $CD4^+$ T cells, and $CD8^+$ T cells. Given (a) the prominence of the decreased NK cell p-PLCγ2 in the identified stratifying features (4 of 12) in the Citrus analysis (Figure 2D) and (b) that NK cell PLCγ2 phosphorylation comprised the top 3 out of 9 significant differences identified in 897 features using 2-tailed Welch's t tests with stringent Bonferroni correction (Supplemental Table 2), hypophosphorylation of PLCγ2 in NK cells appears to be the most important signaling difference distinguishing treatment-naive JDM patients from controls. Dysregulation of PLCγ2 in JDM has not been previously reported, to our knowledge.

NK cell percentages in the blood were decreased in treatment-naive JDM patients in comparison with controls, with a trend toward normalization with the cessation of active disease. Previous work suggested that NK cells may be enriched in affected muscles of JDM patients with short disease duration at diagnosis in comparison with patients with longer disease duration (15), raising the possibility that NK cells may migrate from the blood to affected muscles early in the JDM disease course. Despite the paucity of NK cells in the peripheral blood, NK cells from treatment-naive JDM patients were more highly activated and proliferating to a greater extent than NK cells from healthy controls, as assessed by CD69 and Ki-67, respectively. Interestingly, decreased NK cell frequencies observed in treatment-naive JDM patients correlated with lower levels of PLCγ2 phosphorylation (Supplemental Figure 4). In contrast, NK cell frequency was not correlated with PLCγ2 phosphorylation in JDM patients with clinically inactive disease or in healthy controls (Supplemental Figure 4).

Treatment-naive JDM patient NK cells exhibited lower levels of PLCγ2 phosphorylation than healthy controls at all stimulation time points. Phosphorylation of the upstream kinases Syk/ZAP70 and Itk/Btk in the PLCγ2 signaling cascade was not different between JDM patients and controls, suggesting that PLCγ2 hypophosphorylation is due to other factors (e.g., inhibitory molecules), although the dynamic range of Syk/ZAP70 and Itk/Btk signaling necessary for normal phosphorylation of PLCγ2 is not well established. Minimal differences were seen in PLCγ2 phosphorylation based on the presence of myositis-specific antibodies (Supplemental Figure 3). Interestingly, the 3 patients with no myositis-specific antibodies had the lowest levels of p-PLCγ2, although we did not have enough statistical power to detect a significant difference.

PLCγ2 hypophosphorylation after receptor cross-linking resulted in substantially suppressed calcium flux in treatment-naive patients compared with controls. Cross-linking of 2B4 and NKG2D receptors leads to synergistic, selective PLCγ2 phosphorylation and calcium mobilization (33). No differences were observed in expression levels of 2B4 and NKG2D receptors between treatment-naive JDM patients and controls. PLCγ2 phosphorylation results in a conformational change in PLCγ2, facilitating the hydrolysis

of the membrane phospholipid phosphatidylinositol 4,5-bisphosphate to inositol triphosphate (IP3) and diacylglycerol. IP3 subsequently binds to its receptor on the endoplasmic reticulum and releases cellular stores of calcium. Decreased calcium flux is associated with altered cytotoxic granule movement and localization to the immune synapse, resulting in poor NK cell–mediated killing (22). Therefore, the PLCγ2 hypophosphorylation and decreased calcium flux observed in the JDM patients suggests that NK cells from treatment-naive JDM patients would have decreased NK cell cytotoxicity. This is supported by prior observations of decreased NK cell cytotoxicity in small cohort of 5 JDM patients (27) and a second small study with 5 untreated patients with dermatomyositis (2 of whom were adolescents with JDM) who were found to have low NK cell cytotoxicity compared with controls (28).

After our analysis was completed, we determined that patient 7 had given informed consent during his initial hospitalization, but his study blood sample was not drawn until his first clinic visit 5 weeks later. He was inadvertently included in our analysis as a treatment-naive patient despite having received methylprednisolone (2 mg/kg i.v. for 3 days) followed by oral prednisolone (0.8 mg/kg titrated down to 0.4 mg/kg over 5 weeks) and subcutaneous methotrexate (12 mg/m^2/wk). Surprisingly, his PLCγ2 phosphorylation at all 3 time points was not substantially different from the 16 treatment-naive patients (Supplemental Figure 6A). Indeed, the PLCγ2 phosphorylation of patient 7 (who was MDA5$^+$) looked quite similar to the 9 p155/140 antibody–positive JDM patients (Supplemental Figure 3B). In contrast, for reasons that are not yet clear, his p-MAPKAPK2 had normalized. This finding will be investigated in future studies and may provide insight into JDM response to therapy. To assess whether the inclusion of patient 7 in the treatment-naive cohort had skewed our results, we repeated individual 2-tailed Welch's *t* tests with Bonferroni correction (accounting for 897 comparisons between the 2 groups) without patient 7. This stringent statistical test identified that 3 of the top 4 most significant features (phosphoprotein in a specific immune cell subset) between the JDM patient and control groups were NK cell p-PLCγ2 at 0, 3, and 15 minutes and that 7 of the 8 features that were significantly different between the groups involved p-PLCγ2 (including all 3 time points in nonclassical monocytes), with the other significant feature involving p-MAPKAPK2 in nonclassical monocytes (data not shown) — nearly identical to our findings in the initial cohort (which included patient 7; Supplemental Table 2). Therefore, the inclusion of this new-onset patient (who had started therapy) did not substantially alter our results, and his results suggest that early therapy with corticosteroids and methotrexate is insufficient to attenuate the dysregulated NK cell p-PLCγ2 seen in treatment-naive JDM.

Interestingly, several of the immune cell percentages or signaling differences in JDM patients (e.g., NK cell percentages in JDM patients) were partially attenuated with cessation of active disease. Indeed, PLCγ2 and downstream MAPKAPK2 phosphorylation were substantially increased in NK cells of patients with clinically inactive disease in comparison with those from treatment-naive patients. For 7 of 11 paired treatment-naive patient and clinically inactive disease patient samples, CD16 receptor expression levels also increased with the cessation of active disease (Figure 4E). The attenuation of NK cell defects in patients with clinically inactive disease strongly suggests that the PLCγ2 hypophosphorylation is not due to mutations in PLCγ2.

The mechanism(s) underlying the NK cell PLCγ2 hypophosphorylation in treatment-naive JDM patients is not yet clear. No differences were detected in total PLCγ2 protein level (in a small subset of available patient samples). SHIP1, a negative regulator of p-PLCγ2, was also assessed, and SHIP1 levels were actually lower in NK cells from treatment-naive JDM patients compared with controls, which would not explain the hypophosphorylation of PLCγ2 in NK cells observed in these patients. CD16 expression was lower in JDM patients, but this appears to be correlative rather than causative because signaling through other NK cell receptors (2B4 and NKG2D with normal expression levels) manifested with decreased calcium flux. Future work will leverage RNA-Seq on sorted NK cells (from treatment-naive JDM patients and controls) to further delineate potential inhibitors and other PLCγ2 signaling cascade components that contribute to differences in NK cell PLCγ2 phosphorylation in the early, active JDM environment as well as the impact of the inflammatory environment in JDM on longitudinal changes in PLCγ2 phosphorylation over the course of the disease.

PLCγ2 phosphorylation was also lower in treatment-naive JDM unstimulated classical monocytes. Macrophage CSF-induced monocyte differentiation is mediated through PLCγ2 phosphorylation (34, 35). However, we did not observe perturbations in the percentage of circulating monocytes in treatment-naive JDM patients compared to controls. Only a limited number of prior studies have examined classical monocytes in JDM (13, 36). Future work will evaluate monocyte function to determine if hypophosphorylation of PLCγ2 in classical monocytes has functional significance in these patients.

Although new insights into NK cell PLCγ2 signaling defects in JDM were gained in this study, there were several limitations in this work, including the size of the treatment-naive patient cohort and the number of available PBMCs. The study included 17 treatment-naive patient samples from 2 medical centers and highlights the need for increased collaboration among pediatric centers to obtain enough patients to study new-onset, treatment-naive JDM patients in a statistically meaningful way. To maximize insights from small-volume patient samples, the mass cytometry samples were stimulated with a combination of different stimuli at 3 time points. However, the limited patient samples coupled with a paucity of NK cells in many of the JDM samples restricted the potential of follow-up experiments to assess the functional impact of hypophosphorylation of NK cells' PLCγ2.

A better understanding of the etiology of JDM may inform new targeted therapeutic interventions (e.g., small molecules or biologics that target specific signaling pathways). This study highlighted the utility of mass cytometry coupled with multiparameter phospho-specific antibodies in identifying differences in signaling phenotype in small biological samples from treatment-naive JDM patients and controls. Treatment-naive JDM patient NK cells hypophosphorylated PLCγ2, which resulted in decreased calcium flux, providing a mechanistic explanation for previous reports of poor NK cell killing in JDM patients. Future studies will focus on mechanisms underlying the NK cell PLCγ2 signaling defects in new-onset, treatment-naive JDM patients and on potential strategies to mitigate this signaling defect.

Methods

Patients. JDM was defined according to modified Bohan and Peter's criteria (1). JDM patients diagnosed in our pediatric rheumatology clinics at St. Louis Children's Hospital (site 1) or Ann & Robert H. Lurie Children's Hospital of Chicago (site 2) were eligible for enrollment if their cases were new onset and treatment naive. The definition of clinically inactive disease varied slightly between the two sites. Site 1 defined clinically inactive disease as no proximal muscle weakness, no difficulty swallowing, and only residual Gottron's papules or rash. Site 2 defined apparently inactive disease as a disease activity score (37) of 2 or less.

Reagents. Antibodies conjugated to heavy metals were purchased from Fluidigm, with the exception of CD69 (Supplemental Table 1).

Sample preparation and collection. Blood samples were collected from 17 treatment-naive, new-onset JDM patients, 11 of these 17 JDM patients after achieving clinically inactive disease, and 17 healthy controls (Table 1), and PBMCs were isolated using a Ficoll-Paque PLUS gradient (GE Healthcare) and cryopreserved.

Mass cytometry. PBMCs were thawed and labeled with cisplatin to distinguish live cells (Fluidigm). Cells were aliquoted (1.7×10^6 to 3.3×10^6 cells per tube) into polypropylene tubes with 80 μl volume. Cells were stained with all surface marker antibodies except CD45, CD45RA, and CD45RO for 30 minutes at 37°C, washed with warm media, and rested for 30 minutes at 37°C before stimulation. To maximize insights gained from limited samples, a combination of stimuli to activate different signaling pathways was chosen to stimulate the samples. Cells were left unstimulated or stimulated with 500 U/ml IL-2 (R&D Systems), 50 ng/ml IL-12 (R&D Systems), 500 ng/ml LPS (InvivoGen), 500 U/ml IFN-α4 (PBL InterferonSource), and 1 μl/ml anti-mouse IgG (BioLegend) for 3 or 15 minutes in RPMI1640 medium (Sigma-Aldrich) supplemented with 10% fetal calf serum at 37°C, then fixed with MaxPar Fix I Buffer, permeabilized with MaxPar Barcode Perm Buffer, and barcoded with the Cell-ID 20-Plex Pd Barcoding Kit (Fluidigm). Barcoded samples were pooled and stained with antibodies for CD45, CD45RA, and CD45RO (Supplemental Table 1). After staining for surface markers, the pooled samples were methanol permeabilized and stained with antibodies for intracellular markers (Supplemental Table 1). Samples were put in Cell-ID Intercalator-Ir (Fluidigm) overnight to facilitate detection of debris and doublets and then run on a CyTOF2/Helios instrument (Fluidigm). Samples were debarcoded using the Single Cell Debarcoder, a standalone MATLAB application (38). Data were analyzed using Cytobank and R. A run control from the same normal donor was used in each experiment to normalize the phosphoprotein data as follows:

Data normalization: $\text{arcsinh}(x_{\text{sample}}/5) - \text{arcsinh}(x_{\text{run control}}/5)$ (Equation 1).

Citrus. Citrus, a computational technique combining hierarchical clustering with an analysis of stratifying differences in cluster features (i.e., phosphorylation signaling proteins in immune subsets) between 2 groups of samples, was performed with the R Citrus package on flow cytometry standard files gated on live immune cells to compare treatment-naive patients with healthy controls for each stimulation time point (30). Surface markers were clustering parameters. Minimum cluster size was set as 2% of the total

population, with 10,000 events sampled per file. Cluster characterization features were signaling molecules. All clustering and characterization features were arcsinh transformed. Differences in cluster features were calculated using LASSO feature selection because the number of stratifying features with SAM was too large to manually interpret. LASSO model cross-validation error rates were acceptably low for model interpretation (Supplemental Figure 2).

To aid in interpretation of cluster cell type, all surface marker–transformed medians (Supplemental Table 1) were visualized in a heat map. A PLS-DA model to classify treatment-naive patients from controls was constructed with LASSO-selected features in Citrus, combining all 3 stimulation time points into a single *Z* score–transformed matrix for analysis.

Flow cytometry to assess total PLCγ2 and SHIP1 protein levels in NK cells. Flow cytometry was performed on a subset of 3 treatment-naive patients (for which samples were available) and 3 matched controls collected at the host site to assess total PLCγ2 and SHIP1 levels. Samples (2×10^5 cells per sample) were stained with surface marker antibodies and fixed with Cytofix/Cytoperm buffer (BD Biosciences). Samples were stained with CD16 (3G8) V500, CD3 (UCHT1) PerCP-Cy5.5, CD19 (SJ25C1) BV786, and total PLCγ2 (K86-1161) PE (BD Biosciences), as well as CD56 Pacific Blue (NCAM1), CD45RA (HI100) PE-Cy7, and SHIP1 (P1C1-A5) AF647 (BioLegend). Flow cytometry was performed on a 12-color LRSFortessa X-20 flow cytometer (BD Biosciences) and analyzed with FlowJo (FlowJo, LLC). NK cells were gated as $CD56^+CD3^-$ lymphocytes and analyzed for differences in PLCγ2 and SHIP1 between patient and control samples.

Analysis of NK cell calcium flux via flow cytometry. To assess if differences in NK cell PLCγ2 phosphorylation led to functional alterations, flow cytometry–based calcium flux assays were performed on 2 treatment-naive patients and a control sample. NK cells were enriched using an EasySep Human NK Cell Isolation Kit (STEMCELL Technologies) (>86% purity), then loaded with Indo-1 dye (Invitrogen), and labeled with mouse IgG antibodies against the NK cell receptors 2B4 (clone C1.7, BioLegend) and NKG2D (clone 1D11, BD Biosciences). Kinetic measurements of calcium flux were obtained using a BD LRSFortessa X-20 flow cytometer at baseline and then upon antibody cross-linking using anti-mouse IgG.

Statistics. An α value of 0.05 was set to determine significance, incorporating multiple hypothesis correction as appropriate. Error bars in figures represent the mean plus or minus the SEM. Differences in immune cell proportions were assessed by 1-way ANOVA with Bonferroni's correction for multiple comparisons. Signaling differences in canonically gated cell types were confirmed with 2-tailed Welch's *t* tests with a Bonferroni adjustment to account for testing 897 hypotheses (3 time points with 299 signals in different cell types per each time point). Differences in PLCγ2, Itk/Btk, Syk/ZAP70, and MAPKAPK2 signaling time courses between treatment-naive patients and controls were compared using a 2-tailed Welch's *t* test with Benjamini-Hochberg multiple hypothesis correction ($n = 3$ time points × 4 signaling molecules = 12 hypotheses). Differences in NK cell activation and proliferation (assessed by CD69 and Ki-67, respectively) between treatment-naive patients and controls were assessed using 2-tailed Student's *t* tests with Benjamini-Hochberg multiple hypothesis correction. PLCγ2 flow cytometry panel data were analyzed using 2-tailed Student's *t* tests with Benjamini-Hochberg multiple hypothesis correction to account for testing 2 hypotheses.

Study approval. The study was approved by the institutional review boards at Washington University School of Medicine, St. Louis (IRB ID 201109216), and at Ann & Robert H. Lurie Children's Hospital of Chicago (IRB ID 2008-13457 and 2001-11715), and written informed consent was received to use patient samples.

Author contributions

AAT and ARF wrote the manuscript. AAT, JBA, LMP, and ARF edited the manuscript. LMP provided reagents and samples. AAT, JBA, and ARF designed the research studies. AAT, JBA, ALD, and JTP conducted experiments. AAT, JBA, and ARF analyzed and interpreted data.

Acknowledgments

We would like thank our patients for their participation, without which this work would not be possible. We would also like to thank David Hunstad and Nermina Saucier for critical reading of this manuscript. Technical support was provided by the Immunomonitoring Laboratory at Washington University, which is supported by the Andrew M and Jane M Bursky Center for Human Immunology and Immunotherapy Programs. This research was supported by a Strategic Pharma-Academic Research Consortium grant (to ARF) and National Institute of Allergy and Infectious Diseases R01 AI078994 (to ARF) as well as grants from Cure JM Foundation (to LMP).

Address correspondence to: Anthony R. French, Department of Pediatrics, Washington University, Box 8208, 660 South Euclid Avenue, St. Louis, Missouri 63110, USA. Phone: 314.286.2885; Email: french_a@wustl.edu.

1. Rider LG, Lindsley C, Miller FW. Juvenile dermatomyositis. In: Petty R, Laxer R, Lindsley C, Wedderburn L, eds. *Textbook of Pediatric Rheumatology*. 7th ed. Philadelphia, Pennsylvania, USA: Elsevier; 2016:351–383.
2. Pachman LM, et al. TNFalpha-308A allele in juvenile dermatomyositis: association with increased production of tumor necrosis factor alpha, disease duration, and pathologic calcifications. *Arthritis Rheum*. 2000;43(10):2368–2377.
3. Rider LG, et al. The myositis autoantibody phenotypes of the juvenile idiopathic inflammatory myopathies. *Medicine (Baltimore)*. 2013;92(4):223–243.
4. Pachman LM, Khojah AM. Advances in Juvenile Dermatomyositis: Myositis Specific Antibodies Aid in Understanding Disease Heterogeneity. *J Pediatr*. 2018;195:16–27.
5. Cooper MA, Willingham DL, Brown DE, French AR, Shih FF, White AJ. Rituximab for the treatment of juvenile dermatomyositis: a report of four pediatric patients. *Arthritis Rheum*. 2007;56(9):3107–3111.
6. Aggarwal R, Loganathan P, Koontz D, Qi Z, Reed AM, Oddis CV. Cutaneous improvement in refractory adult and juvenile dermatomyositis after treatment with rituximab. *Rheumatology (Oxford)*. 2017;56(2):247–254.
7. Aggarwal R, et al. Predictors of clinical improvement in rituximab-treated refractory adult and juvenile dermatomyositis and adult polymyositis. *Arthritis Rheumatol*. 2014;66(3):740–749.
8. Miller FW, et al. Genome-wide association study identifies HLA 8.1 ancestral haplotype alleles as major genetic risk factors for myositis phenotypes. *Genes Immun*. 2015;16(7):470–480.
9. Rothwell S, et al. Dense genotyping of immune-related loci in idiopathic inflammatory myopathies confirms HLA alleles as the strongest genetic risk factor and suggests different genetic background for major clinical subgroups. *Ann Rheum Dis*. 2016;75(8):1558–1566.
10. Miller FW, et al. Genome-wide association study of dermatomyositis reveals genetic overlap with other autoimmune disorders. *Arthritis Rheum*. 2013;65(12):3239–3247.
11. Morita R, et al. Human blood CXCR5(+)CD4(+) T cells are counterparts of T follicular cells and contain specific subsets that differentially support antibody secretion. *Immunity*. 2011;34(1):108–121.
12. López de Padilla CM, et al. Plasmacytoid dendritic cells in inflamed muscle of patients with juvenile dermatomyositis. *Arthritis Rheum*. 2007;56(5):1658–1668.
13. Nistala K, et al. Myeloid related protein induces muscle derived inflammatory mediators in juvenile dermatomyositis. *Arthritis Res Ther*. 2013;15(5):R131.
14. Sanner H, Schwartz T, Flatø B, Vistnes M, Christensen G, Sjaastad I. Increased levels of eotaxin and MCP-1 in juvenile dermatomyositis median 16.8 years after disease onset; associations with disease activity, duration and organ damage. *PLoS One*. 2014;9(3):e92171.
15. Pachman LM, Fedczyna TO, Lechman TS, Lutz J. Juvenile dermatomyositis: the association of the TNFα-308A allele and disease chronicity. *Curr Rheumatol Rep*. 2001;3(5):379–386.
16. Mamyrova G, et al. Cytokine gene polymorphisms as risk and severity factors for juvenile dermatomyositis. *Arthritis Rheum*. 2008;58(12):3941–3950.
17. Yokoyama WM, Kim S, French AR. The dynamic life of natural killer cells. *Annu Rev Immunol*. 2004;22:405–429.
18. Caligiuri MA. Human natural killer cells. *Blood*. 2008;112(3):461–469.
19. Orange JS. Natural killer cell deficiency. *J Allergy Clin Immunol*. 2013;132(3):515–525.
20. Caraux A, et al. Phospholipase C-γ2 is essential for NK cell cytotoxicity and innate immunity to malignant and virally infected cells. *Blood*. 2006;107(3):994–1002.
21. Tassi I, Presti R, Kim S, Yokoyama WM, Gilfillan S, Colonna M. Phospholipase C-gamma 2 is a critical signaling mediator for murine NK cell activating receptors. *J Immunol*. 2005;175(2):749–754.
22. Mace EM, et al. Cell biological steps and checkpoints in accessing NK cell cytotoxicity. *Immunol Cell Biol*. 2014;92(3):245–255.
23. Fogel LA, Yokoyama WM, French AR. Natural killer cells in human autoimmune disorders. *Arthritis Res Ther*. 2013;15(4):216.
24. Gianchecchi E, Delfino DV, Fierabracci A. NK cells in autoimmune diseases: Linking innate and adaptive immune responses. *Autoimmun Rev*. 2018;17(2):142–154.
25. O'Gorman MR, Bianchi L, Zaas D, Corrochano V, Pachman LM. Decreased levels of CD54 (ICAM-1)-positive lymphocytes in the peripheral blood in untreated patients with active juvenile dermatomyositis. *Clin Diagn Lab Immunol*. 2000;7(4):693–697.
26. Ernste FC, Crowson CS, de Padilla CL, Hein MS, Reed AM. Longitudinal peripheral blood lymphocyte subsets correlate with decreased disease activity in juvenile dermatomyositis. *J Rheumatol*. 2013;40(7):1200–1211.
27. Miller ML, Lantner R, Pachman LM. Natural and antibody-dependent cellular cytotoxicity in children with systemic lupus erythematosus and juvenile dermatomyositis. *J Rheumatol*. 1983;10(4):640–642.
28. Gonzalez-Amaro R, Alcocer-Varela J, Alarcón-Segovia D. Natural killer cell activity in dermatomyositis-polymyositis. *J Rheumatol*. 1987;14(2):307–310.
29. Tang J, Salem A, Liu H. *Feature Selection For Classification: A Review*. Boca Raton, Florida, USA: CRC Press; 2014:1–25.
30. Bruggner RV, Bodenmiller B, Dill DL, Tibshirani RJ, Nolan GP. Automated identification of stratifying signatures in cellular subpopulations. *Proc Natl Acad Sci U S A*. 2014;111(26):E2770–E2777.
31. Tibshirani R. Regression shrinkage and selection via the lasso. *J R Statist Sov B*. 1996;58:267–288.
32. Asthagiri AR, Reinhart CA, Horwitz AF, Lauffenburger DA. The role of transient ERK2 signals in fibronectin- and insulin-mediated DNA synthesis. *J Cell Sci*. 2000;113(pt 24):4499–4510.
33. Kim HS, Das A, Gross CC, Bryceson YT, Long EO. Synergistic signals for natural cytotoxicity are required to overcome inhibition by c-Cbl ubiquitin ligase. *Immunity*. 2010;32(2):175–186.
34. Obba S, et al. The PRKAA1/AMPKα1 pathway triggers autophagy during CSF1-induced human monocyte differentiation and

is a potential target in CMML. *Autophagy*. 2015;11(7):1114–1129.
35. Bourgin-Hierle C, Gobert-Gosse S, Thérier J, Grasset MF, Mouchiroud G. Src-family kinases play an essential role in differentiation signaling downstream of macrophage colony-stimulating factor receptors mediating persistent phosphorylation of phospholipase C-gamma2 and MAP kinases ERK1 and ERK2. *Leukemia*. 2008;22(1):161–169.
36. Liphaus BL, et al. Increased soluble cytoplasmic Bcl-2 protein serum levels expression decreased Fas expression in lymphocytes monocytes in juvenile dermatomyositis [published online ahead of print August 1, 2018]. *J Rheumatol.* https://doi.org/10.3899/jrheum.171248.
37. Bode RK, Klein-Gitelman MS, Miller ML, Lechman TS, Pachman LM. Disease activity score for children with juvenile dermatomyositis: reliability and validity evidence. *Arthritis Rheum*. 2003;49(1):7–15.
38. Zunder ER, et al. Palladium-based mass tag cell barcoding with a doublet-filtering scheme and single-cell deconvolution algorithm. *Nat Protoc*. 2015;10(2):316–333.